Photodissociation Dynamics of Ethyltoluene and *p*-Fluoroethylbenzene at 193 and 248 nm

Cheng-Liang Huang,[†] Yuri A. Dyakov, S. H. Lin,[‡] Yuan T. Lee,[‡] and Chi-Kung Ni*[,§]

Institute of Atomic and Molecular Sciences, Academia Sinica, P. O. Box 23-166, Taipei, 10617 Taiwan

Received: February 2, 2005; In Final Form: April 19, 2005

Photodissociation of jet-cooled *o*-, *m*-, and *p*-ethyltoluene and *p*-fluoroethylbenzene at both 193 and 248 nm was studied separately using vacuum ultraviolet photoionization/multimass ion imaging techniques. Dissociation occurs exclusively through alkyl chain C−C bond cleavage. The measured photofragment translational energy distributions at 193 nm decrease monotonically with increasing translational energy. The distributions indicate that dissociation occurs from the ground electronic state after internal conversion. However, the photofragment translational energy distributions from *o*-, *m*-, and *p*-ethyltoluene obtained at 248 nm contain a slow and a fast component; the ratios between these components are 1:4, 1:1.3, and 1:6, respectively. On the other hand, only the slow component was observed from *p*-fluoroethylbenzene at 248 nm. The fast components are attributed to the dissociation from the triplet state after intersystem crossing, and the slow components result from the dissociation in the ground electronic state. Comparison with the photodissociation of benzene and toluene and ab initio calculation has been made.

I. Introduction

The quantum yields of fluorescence and phosphorescence, rates of internal conversion and intersystem crossing, and the energy levels of the excited states remain the most important properties in photochemistry. Extensive studies have been focused on the measurement of these properties.

However, even for a molecule as simple as benzene, controversy still remains. For example, the lifetimes and fluorescence quantum yields of the vibrational levels 6^1, 1^16^1, and 1^26^1 in the S_1 states were reported to be 79, 71, 55 ns and 0.27, 0.21, 0.17, respectively. The observed increase in the nonradiative rate with excess energy was ascribed to an enhancement of the $S_1{}^1B_{2u} \rightarrow T_1{}^3B_{1u}$ intersystem crossing.[1] Several possible schemes for mixing of the $S_1{}^1B_{2u}$ and $T_1{}^3B_{1u}$ states were proposed, and many theoretical studies have been reported.[2−7] On the other hand, the lifetimes of several vibronic bands in the S_1 state of benzene were probed in a two-color photoionization/supersonic expansion experiment.[8,9] Biexponential decay curves were observed, and they were assigned as the decays from singlet and triplet states. The vibrational energy dependence of these measurements show that intersystem crossing is dominant in the lower vibrational state and internal conversion becomes the major channel as the vibrational energy increases.[9] This energy dependence of the intersystem crossing rate is totally different from that obtained in fluorescence decay measurement. The recent studies of Doppler-free two-photon excitation (DFTPE) spectroscopy and the Zeeman effect of the $S_1 \leftarrow S_0$ transition of benzene,[10,11] however, suggested another mechanism. In these studies the Zeeman spectra of the 6^1, 1^16^1, and 1^26^1 bands of the $S_1{}^1B_{2u} \leftarrow S_0{}^1A_{1g}$ transition were measured. Many perturbations were observed, and they increase as the excess energy increases. However, all the perturbing levels were found to be a singlet state. No Zeeman splittings which can be attributed to the perturbation from a triplet state were observed. It was suggested that rotationally resolved levels of the S_1 state are not mixed with any triplet state at all. Instead, nonradiative decay of an isolated benzene in the low vibronic states was interpreted as the anharmonic−Coriolis coupling in the S_1 state, and the onset of channel three in benzene occurs via anharmonic−Coriolis coupling in the S_1 state plus internal conversion to S_0.

Compared to benzene, the photochemistry of alkyl-substituted benzenes has received little attention. Early single vibronic level fluorescence spectra studies showed that IVR becomes the dominant process as the alkane chain is increased.[12] Two-color photoionization has been applied to the measurement of the time evolution of laser excited first singlet states of toluene, ethylbenzene, and xylene.[13,14] The observed photoionization signals exhibited a biexponential dependence upon the time delay between the pump and ionization lasers. The fast exponential decay was resulted from the relaxation of the S_1 state, and the slow exponential decay was interpreted as the decay of the T_1 state after the $S_1 \rightarrow T_1$ intersystem crossing. More recent high-resolution laser fluorescence excitation spectra near the band origin of the S_1 state showed that propylbenzene and butylbenzene exhibit the excess absorption line width; however, the source of the excess width remains elusive.[15]

Recently we have applied photofragment translational spectroscopy to study benzene, toluene, xylene, ethylbenzene, and propylbenzene when they were excited to the S_1 and S_2 states.[16−20] These studies show that fast internal conversion to the ground electronic state was the dominant channel for all molecules in the S_2 state. However, the intersystem crossing from S_1 to T_1 becomes the major process for ethylbenzene and propylbenzene when these molecules are excited to the higher vibrational energy levels in the S_1 state.[21,22] In this work, we extend the study to *m*-, *o*-, and *p*-ethyltoluene and *p*-fluoroethylbenzene at both 193 and 248 nm. Different results were found between these molecules. A comparison with benzene and other alkylbenzenes has been made.

* To whom correspondence should be addressed. E-mail: ckni@po.iams.sinica.edu.tw.

[†] Present address: Department of Applied Chemistry, National Chiayi University, Chiayi, 60004 Taiwan.

[‡] Also at: Chemistry Department, National Taiwan University, Taipei, 10617 Taiwan.

[§] Also at: Chemistry Department, National Tsing Hua University, Hsinchu, 30013 Taiwan.

10.1021/jp050571j CCC: $30.25
Published on Web 05/20/2005

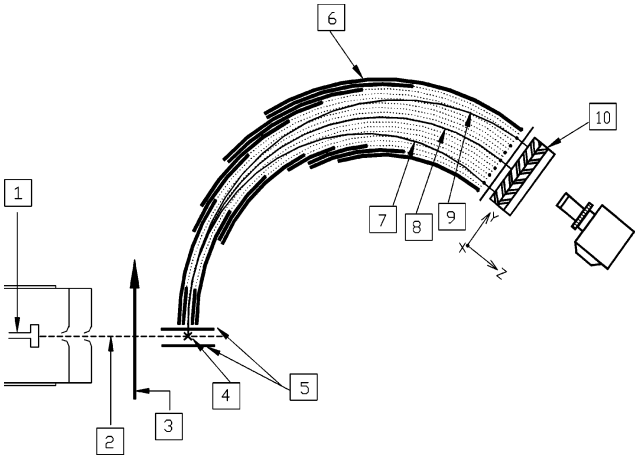

Figure 1. Schematic diagram of the multimass ion imaging detection system: (1) nozzle; (2) molecular beam; (3) photolysis laser beam; (4) vacuum-UV laser beam, which is perpendicular to the plane of the paper; (5) ion extraction plates; (6) cylindrical energy analyzer; (7−9) simulation ion trajectories of $m/e = 16, 14, 12$; (10) two-dimensional detector, where the *Y*-axis is the mass axis and the *X*-axis (perpendicular to the plane of the paper) is the velocity axis.

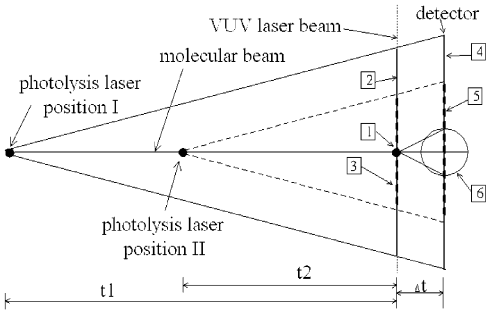

Figure 2. Relationship between the lengths of the images that result from different crossing points of the photolysis laser beam with the molecular beam. The disklike image from the dissociation after ionization is also shown. (1) represents the crossing point of the molecular beam and the vacuum-UV laser beam, where the dissociative ionization occurs. The disklike image, represented by 6 is from the dissociative ionization. (2) and (3) represent the lengths of fragment ion distribution created by vacuum-UV laser photoionization from photolysis laser at position I and position II, respectively. The line shape images, represented by 4 and 5, are from these fragment ion distributions 2 and 3. The t_1 and t_2 represent two different delay times between the photolysis laser pulse and the vacuum-UV laser pulse according to two different photolysis laser positions. Δt is the flight time of the fragment ion in the mass spectrometer.

II. Experiment

The experiments have been described in detail elsewhere,[23] and only a brief description is given here. Ethyltoluene or *p*-fluoroethylbenzene vapor was formed by flowing ultrapure Ar at pressures of 300 Torr through a reservoir filled with liquid sample at 15 °C. The sample/Ar mixture was then expanded through a 500 μm high-temperature (110 °C) pulsed nozzle to form the molecular beam. Molecules in the molecular beam were photodissociated by an UV photolysis laser pulse (Lambda Physik Compex 205; pulse duration $\sim$ 20 ns). Due to the recoil velocity and center-of-mass velocity, the fragments expanded to a larger sphere on their flight to the vacuum-UV laser beam and then were ionized by a vacuum-UV laser pulse. The distance and time delay between the vacuum-UV laser pulse and the photolysis laser pulse were set such that the vacuum-UV laser beam passed through the center-of-mass of the dissociation products and generated a line segment of photofragment ions by photoionization. The length of the segment was proportional to the fragment recoil velocity in the center-of-mass frame multiplied by the delay time between the photolysis and the ionization laser pulses. To separate the different masses within the ion segment, a pulsed electric field was used to extract the ions into a mass spectrometer after ionization. While the mass analysis was being executed in the mass spectrometer, the length of each fragment ion segment continued to expand in the original direction according to its recoil velocity. At the exit port of the mass spectrometer, a two-dimensional ion detector was used to detect the ion positions and intensity distribution. In this two-dimensional detector, one direction was the recoil velocity axis and the other was the mass axis. The schematic diagram of the experimental setup is shown in Figure 1.

Depending on the velocity of the molecular beam, it was necessary to change the distance between the photolysis laser beam and the vacuum-UV laser beam to match the delay time between these two laser pulses to ensure that the ionization laser would pass through the center-of-mass of the products. The change of the distance between the two laser beams changed the length of the fragment ion segment in the image. The relationship between the length of the ion image and the position of the photolysis laser is illustrated in Figure 2. If the molecules were not dissociated after the absorption of UV photons, these high internal energy molecules would remain within the molecular beam. They flew with the same velocity (molecular beam velocity) to the ionization region and were ionized by the vacuum-UV laser. The wavelength of the vacuum-UV laser in this experiment was set at 118.2 nm such that the photon energy was only large enough to ionize parent molecules. The dissociation of parent molecule cations would not occur with the energy left after the vacuum-UV laser ionization. However, the dissociation occurred following the vacuum-UV laser ionization for those hot parent molecules, which absorbed UV photon and did not dissociate into fragments before the arrival of vacuum-UV laser. The ion image of the dissociative ionization was different from the image of the dissociation products of neutral parent molecules. Since ionization and dissociation occurred at the same position, the image of dissociative ionization was a 2D projection of the photofragment ion's 3D-recoil velocity distribution. It was a disklike image, rather than a line-shape image. From the shape of the image and its change with the delay time, the image from dissociation of neutral molecules can easily be distinguished from the dissociative ionization image.

Since the intensity of the line-shape image results from the accumulation of the products produced during the time period from the pump pulse to the probe pulse, the ion image intensity distribution is a function of both the fragment recoil velocity distribution and the dissociation rate. Therefore, the analysis of images at several delay times can reveal the information of the velocity distribution and the dissociation rate. Details of these data analyses have been described in a previous study.[22]

III. Results

A. Photodissociation at 248 nm. The photofragment ion images of *o*-ethyltoluene obtained at 248 nm at various delay times are shown in Figure 3a,b. Fragments of $m/e = 105$, 106, and 107 correspond to 2-methylbenzyl radical, $C_6H_4CH_3CH_2$, and its ^{13}C isotopes due to natural abundance. Some impurity of xylene, corresponding to the image of $m/e = 106$ at the center was also observed. The image of fragment $m/e = 105$ has three components. A component located on both wings and a line-shape component superimposed on a disklike component at the

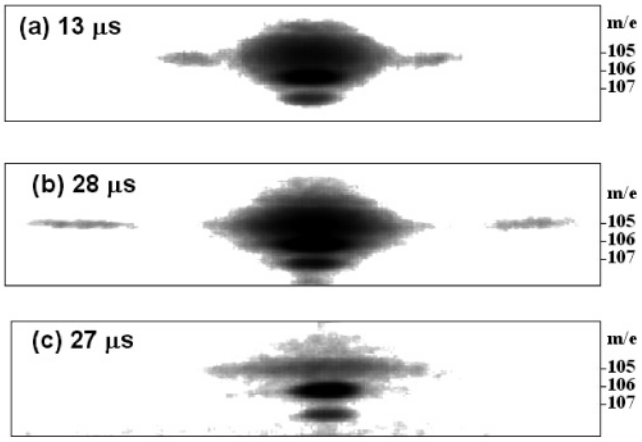

Figure 3. Photofragment ion images from photodissociation at 248 nm: (a) *o*-ethyltoluene at delay time between pump and probe laser, 13 μs; (b) *o*-ethyltoluene, delay time of 28 μs; (c) *p*-fluoroethylbenzene, delay time of 27 μs.

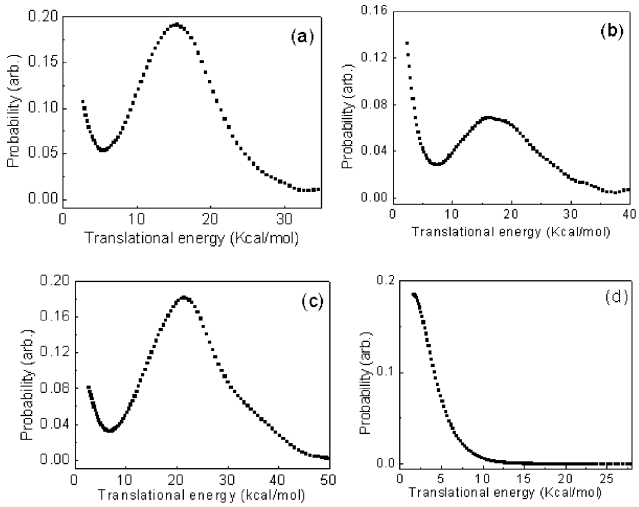

Figure 4. Photofragment translational energy distribution obtained at 248 nm: (a) *o*-ethyltoluene; (b) *m*-ethyltoluene; (c) *p*-ethyltoluene; (d) *p*-fluoroethylbenzene.

center. As the delay time between the pump and the probe laser pulses increased, the component on both wings moved rapidly toward the outside, and the length of the line-shape component at the center increased. On the other hand, the size of the disklike image did not change, but the intensity decreased with the increase of the delay time. These three components can be assigned easily according to the relationship illustrated in Figure 2. The component on the wings and the line-shape component at the center are the 2-methylbenzyl radical fragments that resulted from the dissociation of ethyltoluene with large recoil velocity and small recoil velocity, respectively. The third component, the disklike image, was from the dissociative ionization of undissociated hot ethyltoluene by vacuum-UV photoionization due to the slow dissociation rate at 248 nm.

The photofragment translational energy distribution obtained from the line-shape ion image by forward convolution is shown in Figure 4a. Two components in the photofragment translational energy distribution suggest that there are two mechanisms involved in the dissociation of ethylbenzene at 248 nm. The similar two components in the translational energy distribution were observed from the photodissociation of *m*-ethyltoluene and *p*-ethyltoluene, as illustrated in Figure 4b,c. However, the ratios between these two components are very different. The ratios between slow:fast components change from 1:1.3 for *m*-ethyltoluene to 1:4 and 1:6 for *o*-ethyltoluene and *p*-ethyltoluene, respectively. On the other hand, *p*-fluoroethylbenzene shows a totally different photofragment ion image, as illustrated in Figure 3c. Only one component was observed from the image, and the translational energy distribution decreases monotonically with the increase of the energy, as shown in Figure 4d.

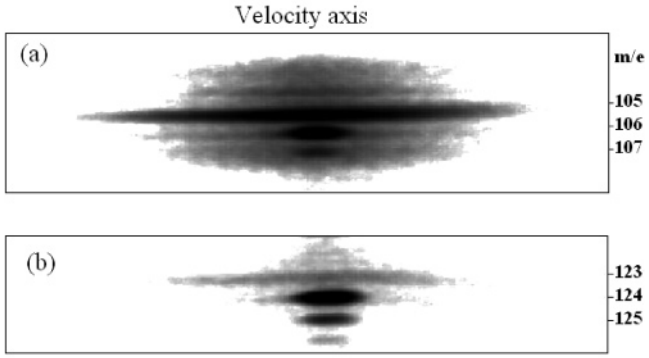

Figure 5. Photofragment ion images from photodissociation at 193 nm: (a) *o*-ethyltoluene, delay time of 26 μs; (b) *p*-fluoroethylbenzene, delay time of 27 μs.

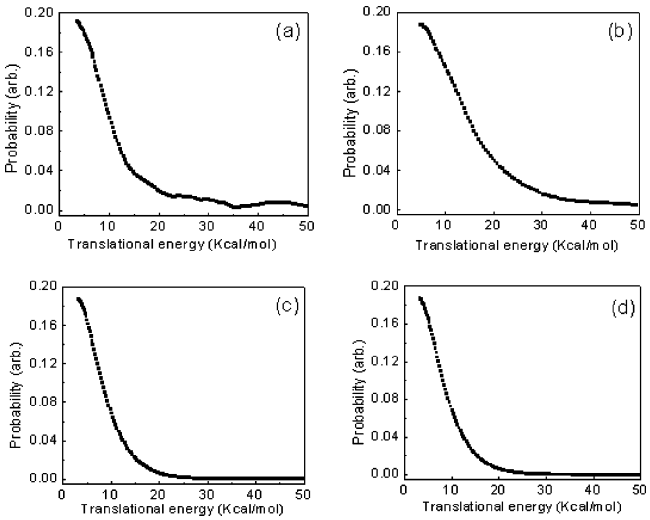

Figure 6. Photofragment translational energy distribution obtained at 193 nm: (a) *o*-ethyltoluene; (b) *m*-ethyltoluene; (c) *p*-ethyltoluene; (d) *p*-fluoroethylbenzene.

B. Photodissociation at 193 nm. The photofragment ion images obtained from the photodissociation of ethyltoluene molecules at 193 nm show very different properties from that obtained at 248 nm. Figure 5a depicts the photofragment ion image obtained from the photodissociation of *o*-ethyltoluene at 193 nm. Only the slow component was observed. On the other hand, the ion image obtained from the dissociation of *p*-fluoroethylbenzene, as shown in Figure 5b, remains the same as that obtained at 248 nm. The fragment translational energy distribution obtained from these ion images are presented in Figure 6.

In the data analysis, we found that the fast components have dissociation lifetimes shorter than 0.1 μs and the slow components have lifetimes longer than 10 μs. The translational energy distributions of each component are not very sensitive to the dissociation lifetime if it is shorter than 0.1 μs or longer than 10 μs. A photolysis laser fluence dependence measurement was carried out in the region of 0.7−10 mJ/cm^2 for 193 nm and 7.8−53 mJ/cm^2 for 248 nm. The shapes and the ratio of these two components in the translational energy distribution do not change with photolysis laser intensity. In addition, the maximum

translational energies are less than the available energies from one-photon dissociation. The measurements suggest that they all result from one-photon dissociation.

IV. Discussion

The photofragment translational energy spectroscopy has been applied to study many aromatic molecules.[17,18] The electronic state on which the dissociation occurs can be identified from the fragment translational energy distributions and dissociation rates. For example, the photodissociation of benzene at 193 and 248 nm has been investigated in a molecular beam. H atom elimination is the only dissociation channel observed at 193 nm. The average translational energy released obtained at 193 nm is very small, and the probability distribution decreases with increasing recoil translational energy. Since there is no exit barrier in the ground electronic state in the dissociation channel $C_6H_6 \rightarrow C_6H_5 + H$, which produces two radicals, the monotonic decrease of the probability with the increasing translational energy must be dissociation from a molecule that has undergone internal conversion to the ground electronic state and subsequently dissociated without encountering an exit barrier. Comparison of the dissociation rates obtained from experimental measurement and RRKM calculation also confirms that dissociation of benzene must occur on the ground electronic state. On the other hand, no dissociation occurs at 248 nm. This can be understood from the fact that the dissociation threshold for H atom elimination (113 kcal/mol) from benzene is almost as high as the photon energy (115 kcal/mol). If there were an excited state with repulsive potential, dissociation would have occurred directly and produced the fragments. However, if internal conversion or intersystem crossing occurs after the excitation, dissociation must be too slow to be observed due to the close values of photon energy and dissociation threshold.

Toluene also shows similar dissociation properties.[19] Absorption of 193 nm corresponds to the excitation to the S_2 state. The translational energy distribution suggests that dissociation occurs after internal conversion to the ground electronic state. The major dissociation channels are the cleavage from the two weakest chemical bonds, $C_6H_5CH_3 \rightarrow C_6H_5CH_2 + H$ and C_6H_5-$CH_3 \rightarrow C_6H_5 + CH_3$. No dissociation was observed at 248 nm. The slow dissociation rate observed at 248 nm also indicates relaxation to lower electronic states after the excitation to S_1 by 248 nm photons.

However, as the length of the alkyl chain increases, the dissociation threshold decreases significantly due to the weak C−C bond in the alkyl chain. Dissociation occurs at both 193 and 248 nm. Dissociation of ethylbenzene and *n*-propylbenzene at 193 nm show a dissociation mechanism similar to that of benzene and toluene; i.e., dissociation occurs in the ground electronic state after internal conversion from the S_2 to S_0 states. However, dissociation from both the ground electronic state and the triplet state after the internal conversion and intersystem crossing were observed at 248 nm. Indeed, more than 70−80% of the excited ethylbenzene and *n*-propylbenzene in the S_1 state dissociate from the triplet state after the intersystem crossing.[21,22]

In this work, we demonstrate that dissociation for ethyltoluene and fluoroethylbenzene at both 193 and 248 nm occur exclusively by the cleavage of the C−C bond in the alkyl chain. Although the products are the same at these two wavelengths, the translational energy distributions were found to be very different for ethyltoluene at these two wavelengths. Since the methyl and ethyl groups and the F atom are not the electronic chromophore at 248 or 193 nm, the photon absorption corresponds to the excitation of the phenyl ring. Dissociation must occur indirectly either through the coupling between the stable and repulsive states or after the internal conversion from the initial excited state to a lower electronic state. Figure 7 shows the potential energy diagram for the CH_3 elimination channel for *o*-, *m*-, and *p*-ethyltoluene and *p*-fluoroethylbenzene obtained from ab initio calculation. In the calculation, the geometries were optimization by B3LYP/6-31G* and the energies were calculated by a G3 scheme. In the ground electronic state, the methyl group changes gradually from pyramidal geometry to planar geometry as the C−C bond length increases during the dissociation process. There is no exit barrier for the dissociation from the ground state. Figure 7 also shows the potential energy diagram in the first triplet state for the same dissociation channel. The exit barrier height is about 26−28 kcal/mol.

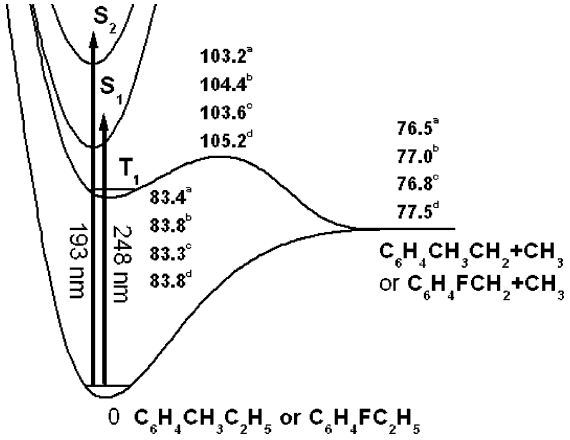

Figure 7. S_0- and T_1-state energy diagrams of CH_3 elimination obtained by ab initio calculation. The numbers are the zero point energies for the S_0 state, the T_1 state, the transition state, and the products. Numbers with superscript a, b, c, and d represent the values of *o*-, *m*-, and *p*-ethyltoluene and *p*-fluoroethylbenzene, respectively.

For ethyltoluene, the translational energy distribution obtained at 193 nm and the slow component obtained at 248 nm decrease monotonically with the increase of energy. The average translational energy release is very small. These are the typical characteristics of the dissociation from the ground electronic state with no exit barrier. In contrast, the fast component of ethyltoluene obtained at 248 nm has a large average released translational energy, and the peak of the distribution is located far from zero. These are characteristics of dissociation from a repulsive excited state or dissociation from an electronic state with an exit barrier. Although the other electronic states cannot be definitively excluded (no potential energy surfaces for the other excited states are available), the exit barrier in the first triplet state and the translational energy distribution of the fast component suggest that dissociation upon intersystem crossing to the first triplet state is a likely explanation for the fast component in the translational energy distribution of ethyltoluene. On the other hand, the translational energy distribution from the dissociation of *p*-fluoroethylbenzene shows similar properties at both 248 and 193 nm; i.e., the probability decreases with the increase of energy, and the average translational energy release is very small. The distributions indicate that the dissociation occurs only in the ground electronic state at both wavelengths. The triplet state does not play a role in *p*-fluoroethylbenzene photodissociation.

Comparison of the photodissociation of ethylbenzene, ethyltoluene, and fluoroethylbenzene in the S_1 state reveals interesting information. When one of the H atoms attached to the aromatic ring of ethylbenzene is replaced by a methyl group, the dissociation dynamics does not change very much. Although

the branching ratios of the dissociation from the ground and the triplet states change with the relative position between ethyl and methyl groups, dissociation from the triplet state after intersystem crossing remains as the major channel for the S_1 state. However, when one H atom of the aromatic ring in ethylbenzene is replaced by an F atom, the dissociation dynamics change significantly. Dissociation occurs exclusively through the ground electronic state. The difference of the dissociation dynamics must be due to the difference in the ratio between the internal conversion rate and the intersystem crossing rate of these molecules. The intersystem crossing is spin-forbidden, and its magnitude increases with the atomic number *Z*. The spin−orbit coupling in an aromatic molecule is increased by the substitution of atoms of higher atomic number, and this increases the probability of triplet−singlet transitions. This phenomenon is known as the heavy atom effect.[24] The heavy atom effect has been observed in Cl, Br, and I substituted aromatic compounds. However, the enhancement effect from an F atom or a methyl group is usually very small, and usually spin−orbit coupling can be neglected. Our experimental data demonstrate the different dissociation dynamics between ethylbenzene, ethyltoluene, and fluoroethylbenzene. It cannot be attributed to the heavy atom effect. However, the source of the difference remains elusive. Further theoretical and experimental investigations are necessary to understand the difference between these molecules.

Acknowledgment. The work was supported by the National Science Council, Taiwan, under Contract NSC 93-2113-M-001-007.

References and Notes

(1) Spears, K. G.; Rice, S. A. *J. Chem. Phys.* **1971**, *55*, 5561−5581.
(2) Parmenter, C. S. *Adv. Chem. Phys.* **1972**, *22*, 365−421.
(3) Avouris, P.; Gelbart, W. M.; El-Sayed, M. A. *Chem. Rev.* **1977**, *77*, 793−833.
(4) Ziegler, L. D.; Hudson, B. S. *Excited States* **1982**, *5*, 41−140.
(5) Lim, E. C. *Adv. Photochem.* **1997**, *23*, 165−211.
(6) Henry, B. R.; Kasha, M. *Annu. Rev. Phys. Chem.* **1968**, *19*, 161−192.
(7) Jortner, J.; Rice, S. A.; Hochstrasser, R. M. *Adv. Photochem.* **1969**, *7*, 149−309.
(8) Duncan, M. A.; Dietz, T. G.; Liverman, M. G.; Smalley, R. E. *J. Phys. Chem.* **1981**, *85*, 7−9.
(9) Otis, C. E.; Knee, J. L.; Johnson, P. M. *J. Phys. Chem.* **1983**, *87*, 2232−2239.
(10) Doi, A.; Kasahara, S.; Kato, H.; Baba, M. *J. Chem. Phys.* **2004**, *120*, 6439−6448.
(11) Wang, J.; Doi, A.; Kasahara, S.; Kato, H.; Baba, M. *J. Chem. Phys.* **2004**, *121*, 9186−9187.
(12) Hopkins, J. B.; Powers, D. E.; Smalley, R. E. *J. Chem. Phys.* **1980**, *72*, 2905−2906. Hopkins, J. B.; Powers, D. E.; Smalley, R. E. *J. Chem. Phys.* **1980**, *72*, 5039−5048. Hopkins, J. B.; Powers, D. E.; Smalley, R. E. *J. Chem. Phys.* **1980**, *73*, 683−687. Hopkins, J. B.; Powers, D. E.; Mukamel, S.; Smalley, R. E. *J. Chem. Phys.* **1980**, *72*, 5049−5061. Mukamel, S.; Smalley, R. E. *J. Chem. Phys.* **1980**, *73*, 4156−4166.
(13) Dietz, T. G.; Duncan, M. A.; Liverman, M. G.; Smalley, R. E. *J. Chem. Phys.* **1982**, *76*, 1227−1232.
(14) Lohmannsroben, H. G.; Luther, K.; Stuke, M. *J. Phys. Chem.* **1987**, *91*, 3499−3503.
(15) Borst, D. R.; Pratt, D. W. *J. Chem. Phys.* **2000**, *113*, 3658−3669. Borst, D. R.; Joireman, P. W.; Pratt, D. W.; Robertson, E. G.; Simons, J. P. *J. Chem. Phys.* **2002**, *116*, 7057−7064.
(16) Huang, C. L.; Jiang, J. C.; Lee, Y. T.; Lin, S. H.; Ni, C. K. *Aust. J. Chem.* **2001**, *54*, 561−571.
(17) Tsai, S. T.; Lin, C. K.; Lee, Y. T.; Ni, C. K. *J. Chem. Phys.* **2000**, *113*, 67−70.
(18) Tsai, S. T.; Huang, C. L.; Lee, Y. T.; Ni, C. K. *J. Chem. Phys.* **2001**, *115*, 2449−2455.
(19) Lin, C. K.; Huang, C. L.; Jiang, J. C.; Chang, A. H. H.; Lee, Y. T.; Lin, S. H.; Ni, C. K. *J. Am. Chem. Soc.* **2002**, *124*, 4068−4075.
(20) Huang, C. L.; Jiang, J. C.; Lee, Y. T.; Ni, C. K. *J. Phys. Chem. A* **2003**, *107*, 4019−4024.
(21) Huang, C. L.; Jiang, J. C.; Lin, S. H.; Lee, Y. T.; Ni, C. K. *J. Chem. Phys.* **2002**, *116*, 7779−7782.
(22) Huang, C. L.; Jiang, J. C.; Lee, Y. T.; Ni, C. K. *J. Chem. Phys.* **2002**, *117*, 7034−7040.
(23) Tsai, S. T.; Lin, C. K.; Lee, Y. T.; Ni, C. K. *Rev. Sci. Instrum.* **2001**, *72*, 1963−1969.
(24) Birks, J. B. *Photophysis of Aromatic Molecules*; John Wiley & Sons Ltd.: London, New York, Sydney, Toronto, 1970.